

Article

The Cooling Effect of an Urban River and Its Interaction with the Littoral Built Environment in Mitigating Heat Stress: A Mobile Measurement Study

Yasha Wang ^{1,*}, Wanlu Ouyang ^{2,3}, Qingming Zhan ^{4,5} and Li Zhang ⁶¹ Faculty of Design and Architecture, Zhejiang Wanli University, Ningbo 315100, China² Department of Building and Real Estate, The Hong Kong Polytechnic University, Hong Kong, China³ Institute of Future Cities, The Chinese University of Hong Kong, New Territories, Hong Kong, China⁴ School of Urban Design, Wuhan University, Wuhan 430072, China⁵ Research Center of Digital City, Wuhan University, Wuhan 430072, China⁶ College of Horticulture and Forestry Sciences, Huazhong Agricultural University, Wuhan 430070, China

* Correspondence: wangyasha@zwu.edu.cn

Abstract: Rivers within urban areas could influence the thermal environment by modifying air temperature (AT) and relative humidity (RH). To further explore the cooling effect of a large river on surrounding urban areas, we conducted mobile measurements near the Yangtze River in Wuhan during a hot and humid summer day. This research examined the river cooling effect, determined the thresholds of the cooling and humidifying distance using a third-order polynomial method, assessed littoral heat stress at the pedestrian level and investigated the impact of the littoral built environment using stepwise regression analysis. The results revealed that (1) the cooling and humidifying effect of the river was up to 3.55 °C, 1741 m and 17.25%, 1369 m in the daytime, which was much greater than that at night; (2) the river significantly mitigated pedestrian heat stress within 1200 m from the riverbank in the daytime, but showed a weak negative effect at night; (3) the built environment has a significant impact on the littoral areas, e.g., urban greening during the daytime and building morphology at night. The findings of this study provide empirical evidence for the cooling effect of a large river in urban areas and further support climate-sensitive planning and design for our thermal environment.

Keywords: field measurement; air temperature; relative humidity; apparent temperature; urban waterbody; urban morphology

Citation: Wang, Y.; Ouyang, W.; Zhan, Q.; Zhang, L. The Cooling Effect of an Urban River and Its Interaction with the Littoral Built Environment in Mitigating Heat Stress: A Mobile Measurement Study. *Sustainability* **2022**, *14*, 11700. <https://doi.org/10.3390/su141811700>

Academic Editor: Baojie He

Received: 9 August 2022

Accepted: 13 September 2022

Published: 18 September 2022

Publisher's Note: MDPI stays neutral with regard to jurisdictional claims in published maps and institutional affiliations.



Copyright: © 2022 by the authors. Licensee MDPI, Basel, Switzerland. This article is an open access article distributed under the terms and conditions of the Creative Commons Attribution (CC BY) license (<https://creativecommons.org/licenses/by/4.0/>).

1. Introduction

Facing the great challenge of climate change [1], urban heat island (UHI) is becoming an urgent topic for the improvement of human habitats. In 2018, more than 55% of the world's population lived in cities [2], and this number is increasing as the urbanization process develops. For the health of urban residents, global cities are facing a pressing need for mitigation and adaptation strategies to alleviate UHI for urban planning and management processes [3–6]. One of the widely applied strategies is to utilize the cooling effect of natural resources (i.e., urban open waterbodies) to improve the thermal environment.

Urban waterbodies have great potential to modify the thermal environment through heat capacity and evaporative processes [7,8]. A large number of studies have demonstrated the thermal impact of open waterbodies on surrounding urban areas in warm seasons. However, conclusions about the cooling provision of urban waterbodies remain controversial in the current literature. For example, some studies observed cooling effects provided by small rivers, i.e., average cooling of nearly 1 °C in the warm season [9] and a maximum of 3 °C in extremely hot weather [10], whereas some studies revealed that open

waterbodies in urban areas could increase, rather than decrease, the UHI effect [11,12]. In general, the water cooling effect is related to the geometric characteristics of the waterbody and is not consistent between day and night [9,13]. So far, there is limited empirical evidence to underpin the argument. In addition, urban waterbodies could decrease temperature and increase humidity simultaneously, having the opposite effect on thermal comfort [11,14]. In extremely hot weather, the assessment of heat stress at the pedestrian level by combining the water cooling effect and humidifying effect is worthy of further attention.

The cooling effect of urban waterbodies has been explored by both remote-sensed land surface temperature [15–18] and ground-observed air temperature [9–11,14,19–21] in previous studies. The data collection methods of ground-based observation in previous studies mainly involved fixed and mobile measurements [22]. Compared with a fixed station, mobile measurement could provide better spatial resolution data at a lower cost. Mobile data collection at the pedestrian level is helpful to acquire “real-world” microclimate parameters and describe accurate thermal conditions that people can feel. Therefore, it has been regarded as a cost-effective method and is being increasingly used to investigate the outdoor thermal environment. A typical case of mobile measurement was conducted near the Cheonggye River and revealed a mean river cooling effect of 0.46 °C, 32.7 m at 2 p.m. and 0.37 °C, 37.2 m at 10 p.m. [23]. Other researchers used mobile measurement to monitor intra-urban air temperature at a micro-scale [24,25], examine the cooling effect of urban green spaces [26,27] and assess the UHI effect inside local climate zones [28,29]. These previous studies confirm the feasibility of using mobile measurement methods for microclimate investigation [30].

The cooling effect of the urban waterbody is also influenced by the characteristics of the littoral built environment, including urban greening and building morphology. On one hand, urban greening could provide a cooling effect during the hot summer season by shading and evapotranspiration [31,32]. The green coverage ratio is one of the main impact factors affecting the cooling provision [33,34] and a 10% increase in tree cover led to a 0.052 °C drop in temperature in Hong Kong [35]. On the other hand, building morphology plays an important role in pedestrian microclimate [36–38]. Previous scholars related the openness of an urban form, which is measured as the sky view factor, with UHI intensity [39,40]. Air temperature was also found to correlate with building morphology, including the indicators of building density [41–43], building height [41,44] and floor area ratio [38,41,44]. In littoral areas, local building environment indicators were found to have an impact on the water cooling effect. For example, since potential cooling by urban greening and waterbodies may jointly modify the temperature and humidity with interactive effects [45], higher vegetation cover in littoral areas has been observed to increase the water cooling effect [9]. Additionally, specific urban forms, including opening up streets to the river [9,46], building narrower streets and positioning lower buildings near the river [23], were revealed to enhance the water cooling effect. Those efforts underlined the thermal impact of the urban built environment in littoral areas and raised the necessity to explore the interactive effects of these factors and water cooling effect in the littoral areas by local observation.

The Yangtze River, the largest river in China, has great cooling potential for the cities it flows through. Wuhan, the most populous city in the middle reaches of the Yangtze River, has a large littoral area and developers are aiming to build a waterfront ecological city. Consequently, this study obtained a mobile measurement near the Yangtze River in Wuhan and aimed to investigate the river cooling effect and the impact of the littoral built environment in the hot summer season. This study aimed to answer two main research questions: How does a large urban river cool the littoral areas? Does the urban built environment have an impact on the water cooling effect? Subsequently, three objectives were raised:

- (1) To reveal the spatial distribution of air temperature (AT) and relative humidity (RH) near the river in the daytime and nighttime;

- (2) To quantify the heat stress conditions by heat index (HI) and its spatial pattern in the littoral area;
- (3) To investigate the impacts of the urban built environment and the distance from the river bank on the water cooling effect within the littoral areas.

2. Materials and Methods

2.1. Study Area and Route Description

Wuhan (29°58′–31°22′ N, 113°41′–115°05′ E) is one of China's megacities and is located in the central region (Figure 1). Over the past decade, rapid urbanization has led to the growing UHI phenomenon, which places Wuhan in top tier of the hottest cities in China. The Koppen Climate Classification is *Cfa*, Humid Subtropical Climate. The average annual temperature is 17.5 °C, the average annual rainfall is 1269 mm and the total annual sunshine hours range from 1810 to 2100 h. The prevailing wind direction is southeast in summer and northwest in winter. Wuhan features a long summer period from June to September, with a maximum temperature of 37–39 °C, abundant rainfall and typically low wind speed. Known as the River City, Wuhan is built along the Yangtze River, which flows through the city with an average width of 1.3 km. Open waterbodies are not only essential for hydrological and carbon cycles [9,23], but also play an important role in regulating urban climate [47].

To investigate the water cooling effect in urban areas, we selected a relatively typical urban area near the Yangtze River to conduct the mobile measurement. The density and height of surrounding buildings are moderate. The survey points arrayed along two routes: Yuanlin road (YL) and Jianshe 1st road (JS). Both start from the riverside and have the same orientation, i.e., approximately perpendicular to the river. The two routes, less than one kilometer from each other, provide 35 survey points within a 1.8 km distance from the riverbank to collect temperature and humidity data. The locations are shown in Figure 1 and the detailed surrounding environment is shown in Figure 2.

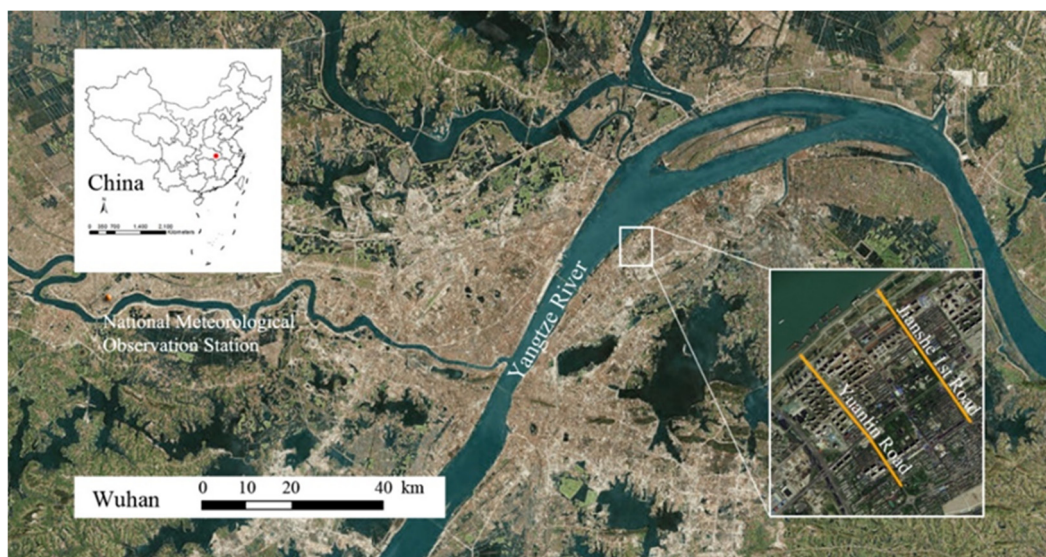


Figure 1. Study area and the measurement routes.

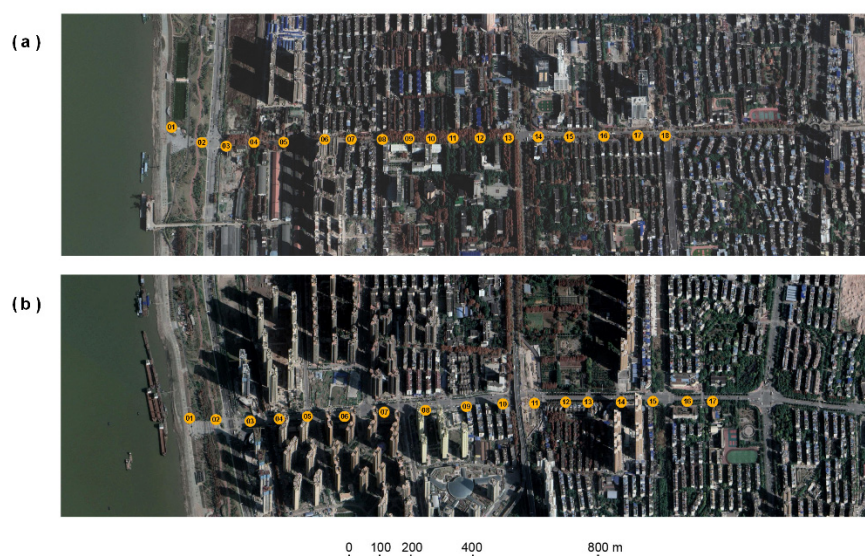


Figure 2. Survey points and the surrounding built environment: (a) Jianshe 1st Road; (b) Yuanlin Road.

2.2. Field Measurements

HOBO U23 Pro V2 data loggers were used to collect air temperature (AT) and relative humidity (RH). The operation ranges were $-40\text{ }^{\circ}\text{C}$ to $70\text{ }^{\circ}\text{C}$ and 0% to 100%, the accuracies were $\pm 0.2\text{ }^{\circ}\text{C}$ and $\pm 2.5\%$ and the resolutions were $0.04\text{ }^{\circ}\text{C}$ and 0.05% , respectively. To avoid direct sunshine, each HOBO sensor was sheltered under a ventilated solar shelter. The sensors were set at a 1.5 m height and logged at a time interval of one second. Meanwhile, a portable GPS device (Magellan eXplorist 310) was used to record the location during the mobile measurement.

The measurement was taken on 21 July 2018, an extremely hot day with a clear sky and calm weather. The average daily temperature was $32.72\text{ }^{\circ}\text{C}$, the maximum temperature was $38.40\text{ }^{\circ}\text{C}$ and the average daily wind speed was 1.50 m/s . The details of the weather conditions are listed in Table A1. The sensors were calibrated before the measurement and the data collected from different routes were corrected using the difference between the calibration values. The mobile measurement was taken during both daytime (9:00–10:30) and nighttime (22:00–23:30). A total of 35 survey points were set in the two routes (Figure 2) and the distances between the points ranged from 50 to 200 m. Between each measurement point, the equipment was ensured to stabilize for at least 20 s; afterwards, it stayed for 2 min for data collection before moving to the next point.

2.3. Survey Data Preprocess

For each point, the data collected in the first 20 s were removed for the stabilized periods, and the data of the remaining 100 s and the last 10 s were then compared. The correlations between these two periods were almost equal, with R^2 above 0.99 and the slope nearly equaling 1 (Figure A1). Therefore, the equipment was deemed to be stabilized and the data during the last 100 s were averaged for each survey point.

To limit the impact of background weather, the duration of each transect measurement was no more than 90 min. Then, we corrected the temporal change of background AT and RH for the transect survey points based on the data from the National Meteorological Observation Station (No. 57494) (Figure 2). The hourly air temperature and relative humidity data on the measurement day were obtained (Table A1) and the measured AT and RH were corrected by a linear detrending for each route [48,49].

2.4. Heat Stress

Then, we further examined the impact of the river on apparent temperature and quantify the littoral heat stress at the pedestrian level. The apparent temperature is affected by air temperature, relative humidity, solar radiation, wind speed, air pressure, clothing condition, etc., and was proposed to assess sultriness in high temperature and humidity conditions [50]. As a simplified version of apparent temperature, Heat Index (HI) has become a popular heat exposure metric in thermal comfort and environmental health [51]. It is a primary indicator used by the US National Weather Service (NWS) because it is closely relevant to heat-related morbidity [52] and it has been employed to investigate thermal comfort in some Chinese cities [20,53]. HI measures how the temperature feels to the human body [54] by combining the effects of air temperature and relative humidity [55]. Focusing on the apparent temperature under a relatively high temperature, high humidity and low wind speed, HI was selected subsequently and calculated as shown in Equation (1) [51]:

$$\begin{aligned} \text{HI} = & -42.379 + 2.04901523 T + 10.14333127 R - 0.22475541 T R - 0.00683783 \\ & T^2 - 0.05481717 R^2 + 0.00122874 T^2 R + 0.00085282 T R^2 - 0.00000199 T^2 R^2 \end{aligned} \quad (1)$$

where T was air temperature (AT in degrees Fahrenheit) and R was the relative humidity (RH) [56].

2.5. The Urban Built Environment

The measured area is located in the southeast of the Yangtze River and all the roads are parallel or vertical to the riverbank (Figure 1). This area is dominated by mid- and high-rise buildings (no more than 100 m), with relatively moderate building density and urban greening. The built environment at the local scale usually includes street location, building geometry and vegetation cover. Since the survey points of this study were distributed in the streets with the same orientation, the impact of the built environment was considered to be mainly from urban greening and building morphology. To quantify the urban greening coverage around the survey points, NDVI-based Fractional Vegetation Cover (FVC) was used. The Sentinel-2A imagery (10 m resolution multispectral) obtained on July 29, 2018, with a cloud cover percentage of 1.59%, was employed to calculate the NDVI. Both the image date and time were very close to that of our field measurement. Therefore, the selected imagery can generally represent the green coverage on the day of the measurement. Initially, the NDVI was calculated as shown in Equation (2):

$$\text{NDVI} = (\text{NIR} - \text{RED}) / (\text{NIR} + \text{RED}) \quad (2)$$

where NIR was the Band 8 (central wavelength 842 nm) of Sentinel-2 and RED was the B4 (central wavelength 665 nm), respectively. Then, the fractional vegetation cover (FVC) was derived by scaling NDVI based on a dense vegetation mosaic-pixel model [57,58], as shown in Equation (3):

$$\text{FVC} = (\text{NDVI} - \text{NDVI}_s) / (\text{NDVI}_v - \text{NDVI}_s) \quad (3)$$

where NDVI_s was the NDVI of bare soil and NDVI_v was the NDVI of pure vegetation.

To quantify the urban morphology, four commonly used indicators were selected from both 2D (two-dimensional) and 3D (three-dimensional) perspectives [40,41,43,44,59–63]. The 2D indicator was building density (BD) and building height (BH). The 3D indicators were sky view factor (SVF) and floor area ratio (FAR). Lan and Zhan [41] revealed that 200 m was an optimal spatial scale for examining the AT–building relationship in Wuhan, so we calculated the morphological indicators at a 200 m scale (i.e., with a buffer radius of 100 m around each point). The details of the indicators and their formula can be found in Table 1.

Table 1. Definition and formula of the selected building morphological indicators.

	Definition	Formula
SVF	Sky View Factor The fraction of the visible sky on a hemisphere of a central point	$SVF = 2\pi - \sum_d^{ND} S_{Hd}$ d is the azimuthal direction (8 as the max); S_{Hd} is the surface of the hemisphere obstructed by buildings in the azimuthal direction d [64]
BD	Building Density The percentage of the land surface covered by buildings	$BD = \frac{\sum_i^n C_i}{C_L}$ C_i is the coverage area of the building; C_L is the land area at a spatial scale of interest
BH	Building Height The area-weighted average height of the buildings	$BH = \frac{\sum_i^n C_i H_i}{C_L}$ C_i is the coverage area of the building; H_i is the height of the building; C_L is the land area in the certain spatial scale
FAR	Floor Area Ratio The ratio between the total floor area and the land area	$FAR = \frac{\sum_i^n C_i * F_i}{C_L}$ C_i is the coverage area of the building; F_i is the number of floors; C_L is the land area in the certain spatial scale

2.6. Data Analysis

A third-order polynomial method was used to determine the maximum distance where the cooling effect of the river could reach [23,65]. The inflexion distance was calculated from the fitting curve of the distance–AT/RH function, which indicated that the microclimatic variables were no longer affected by the river beyond this distance.

To examine the relationship between the microclimate variables and morphological indicators, Pearson correlation and unary linear regression analyses were conducted. Then, taking the microclimatic variables as dependent variables, we used a stepwise multivariable regression model to analyze the potential impact factors, including distance from the riverbank, urban greening and building morphological indicators. The data analysis of this study was conducted in SPSS 22.0 and R version 4.0.0.

3. Results

3.1. The Cooling and Humidifying Effect of the River

As shown in Table 2, AT showed a range of 32.74–36.29 °C in the daytime and a range of 31.23–32.33 °C in the nighttime. The measured daytime RH ranged from 50.82% to 68.07% and the nighttime RH from 63.58% to 71.92%. Overall, the temperature was higher, the humidity was lower, and the standard deviation was larger during the daytime than that during nighttime. Additionally, there was a linear relationship between RH and AT (Figure 3) of the survey points, with the determinate coefficient of 0.907 in the daytime and 0.916 at night. The negative correlation between AT and RH implied simultaneous cooling and humidifying by the river.

Table 2. Statistic summary of measured AT and RH.

		Min	Max	Mean	STD	Range
AT (°C)	Daytime	32.74	36.29	34.72	1.22	3.55
	Nighttime	31.23	32.33	31.86	0.31	1.10
RH (%)	Daytime	50.82	68.07	56.87	5.67	17.25
	Nighttime	63.58	71.92	66.29	2.06	8.34

Note: STD means standard deviation.

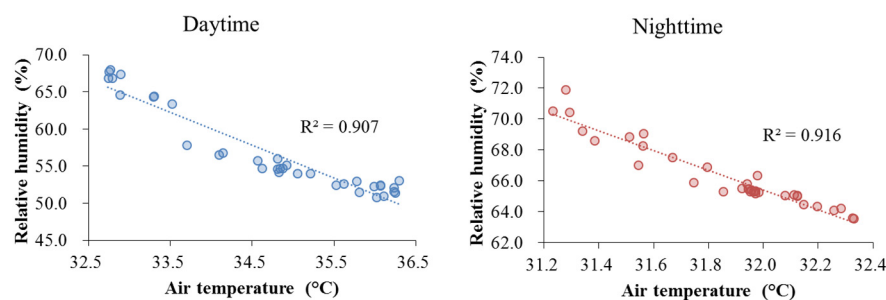


Figure 3. Correlation between relative humidity and air temperature.

Figure 4 described the spatial distribution of littoral AT and RH. With the the distance from the riverbank (DIST) rising, the air temperature increased while the relative humidity decreased. Both AT and RH have cubic polynomial relationships with DIST. A higher coefficient was presented in the daytime for both the DIST–AT relation ($R^2 = 0.936$) and DIST–RH relation ($R^2 = 0.910$) than that in the nighttime (0.734 and 0.855, respectively). The inflexion distances of those cubic polynomial functions, which means the turning point of the curve and the distance of the highest or lowest values, were 1741 m for daytime AT, 1253 m for nighttime AT, 1369 m for daytime RH and 1170 m for nighttime RH. The cooling and humidifying extent during the daytime is much larger than that at night, for instance, the daytime cooling distance is 488 m and the daytime humidifying distance is 199 m farther than nighttime. Those distances indicated the furthest microclimatic influence that the Yangtze River could reach in the selected routes. Therefore, the points located out of the inflexion distances were excluded in the regression analysis in the subsequent multiple regression.

Taking the data from a national weather station in Wuhan (No. 57494) as a reference, we extracted the AT and RH during the hour of the mobile measurement. As shown in Figure 4, the dashed lines represent the background urban climate conditions. The intersection points between the reference line and the measurement trends appeared at around 1100 m for AT and 1000 m for RH in the daytime, which was much further than that in the nighttime, with roughly 400 m and 600 m, respectively. This indicates that, compared to the background weather condition, the cooling effect of the Yangtze River can extend to around 1000 m during the day and about 500 m at night.

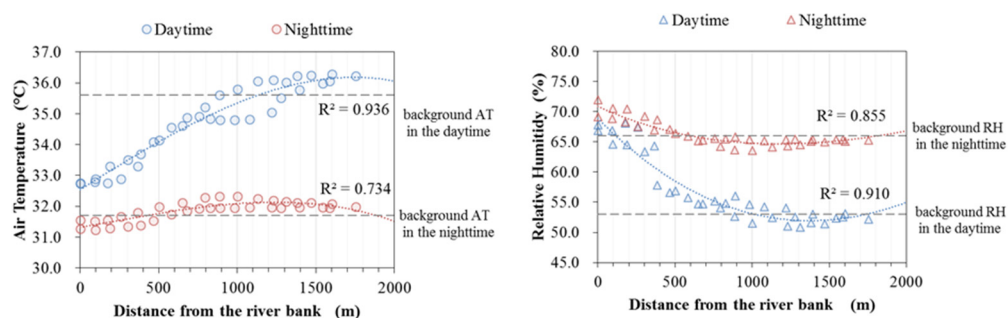


Figure 4. Spatial variation of air temperature and relative humidity.

3.2. Assessment of Littoral Heat Stress

As shown in Figure 3, the AT and RH of the survey points showed a negative relationship, which may exert the opposite effect on the apparent temperature. Therefore, HI, defined as apparent temperature, was selected to assess the heat stress by considering both AT and RH and its spatial variation, as illustrated in Figure 5. HI showed a linear relationship with DIST in the daytime, with the coefficient at 0.738. Similar to Section 3.1, we took the background HI value as a reference line and found that the intersection point

of the daytime appeared at nearly 1200 m, which was close to that of AT and RH. During the nighttime, only a weak correlation between the HI and distance from the riverbank presented, and most of the survey points showed higher HI values than the background reference level. This implied that during the daytime, the temperature reduction from the waterbody could offset the disadvantage of the humidity promotion in the littoral zone. However, at night, humidity promotion played a bigger role and there was a slightly negative effect for littoral heat stress.

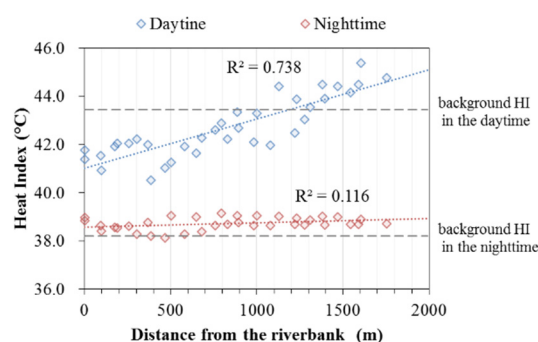


Figure 5. Spatial variation of the heat index.

To further investigate how HI was affected by AT and RH, the relationships between them are plotted in Figure 6. Overall, the AT–HI relations were positive, and the RH–HI relations were negative. Additionally, there were some data points present as outliers during the daytime (Figure 6a,b). These outliers came from the first nine survey points in the near-shore area (Figure 6e). After excluding them, the HI showed a linear relationship with AT ($R^2 = 0.944$) and RH ($R^2 = 0.695$). This pattern persisted during the night, but those nine outlier points had a weaker influence on the correlations. The spatial anomaly may be due to the uneven urban form of the littoral area. The first nine points were located in the areas transecting from the open space near the river to the built environment. There is a green belt and a city road with few buildings along the riverside. The cold, damp air from the Yangtze River spreads to the littoral area and the humidity decreases gradually. Due to the lack of building obstruction, the humidity in the near-shore area is particularly high and led to higher HI values than expected. Since the near-shore area does not have a typical urban built environment, the first nine points were excluded in the regression analysis in the next step. This also underlined the necessity of exploring the impact of the morphological indicators of the built environment on the cooling effect of the urban river.

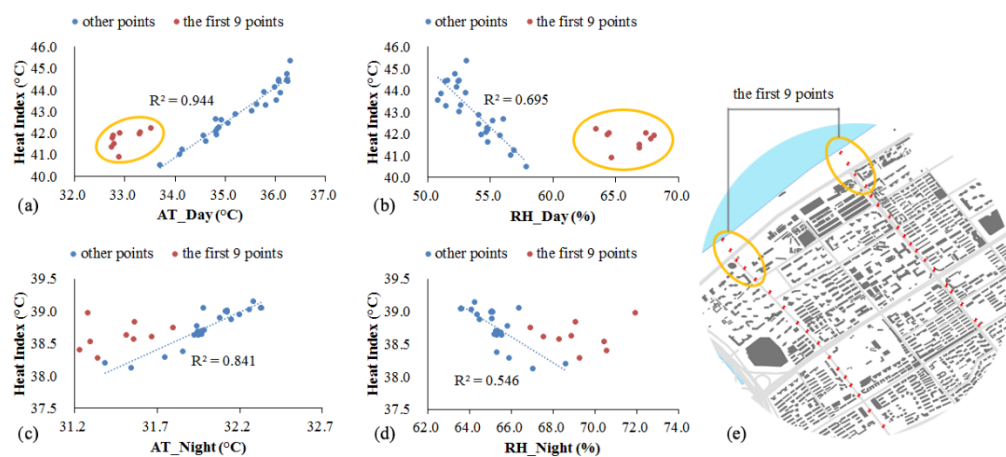


Figure 6. Relationships between HI and AT/RH: (a) HI-AT_Day; (b) HI-RH_Day; (c) HI-AT_Night; (d) HI-RH_Night; (e) location of the first nine survey points. The red dot represents the data of the first nine survey points, and the blue dot represents the data of other survey points.

3.3. Impact of the Urban Built Environment

Table 3 summarized the main features of selected indicators, which describes the morphological conditions of greening and building along the measurement routes. FVC ranged from 0.10 to 0.67, with the regularly planted street trees for the sidewalk, an urban park beside Yuanlin Road and a university campus adjacent to Jianshe Road. As the street width along the survey routes was about 40–60 m, SVF has a mean value of 0.82 and the maximum value, which was obtained at the riverside, was nearly 1.00. BH reached up to 65 m and had an average height of 21.54 m. BD and FAR of the survey site had a mean value of 0.17 and 3.37, respectively, and reached a maximum of 0.33 and 9.12 separately. Considering the potential relations between building morphological indicators, we examined the Pearson correlation coefficients between SVF, BD, BH and FAR (Table 4), and found that FAR significantly correlated with SVF, BD and BH.

Table 3. Statistic of urban greening and morphological indicators.

	Min	Max	Mean	STD
FVC	0.10	0.67	0.29	0.15
SVF	0.63	1.00	0.82	0.11
BD	0.00	0.33	0.17	0.09
BH	0.00	65.40	21.54	17.41
FAR	0.00	9.12	3.37	2.20

Note: STD means standard deviation.

Table 4. Pearson correlation coefficient between SVF, BD, BH and FAR.

	SVF	BD	BH	FAR
SVF	1	−0.328	−0.582 **	−0.747 **
BD	−0.328	1	−0.129	0.350 *
BH	−0.582 **	−0.129	1	0.716 **
FAR	−0.747 **	0.350 *	0.716 **	1

Note: ** significant at 0.01 level (two-tailed). * significant at 0.05 level (two-tailed).

Stepwise multivariable regression analysis was applied to investigate the relationship between the microclimate variables and the built environment features. Other than five indicators of greening and building morphology, DIST was also involved in the analysis. The first nine points in the near-shore area were excluded for their lack of representativeness of the morphological conditions (see Section 3.2), and the points exceeding the inflexion distance were also not included because they were out of the impact zone of the Yangtze River (see Section 3.1). Consequently, the regression analysis involved 25 points for daytime AT, 17 points for nighttime AT, 19 points for daytime RH, 15 points for nighttime RH and 26 points for daytime HI, respectively. Nighttime HI is not presented here, as it showed no apparent variations along with the routes at night, which is illustrated in Section 3.2.

The regression result presented in Table 5 showed that DIST was the dominant factor to influence AT and RH in both the daytime and nighttime. This reconfirmed the significant cooling effect of the large river. Among the selected indicators, FVC, together with DIST, played an important role in the daytime with the adjusted R^2 of 0.831 for AT and 0.820 for RH. In the nighttime, FAR and DIST affected both AT and RH, with the adjusted R^2 being 0.685 and 0.897, respectively. Similar to AT and RH, daytime HI was mainly influenced by DIST and FVC with the adjusted R^2 of 0.821. Although the littoral thermal environment is complex and dynamic, the regression results indicated the urban built environment has significant impact on the cooling and humidifying effect of the urban river.

Table 5. Multiple regression results.

		Unstandardized Coefficients		Standardized Coefficients	t	p-Value	Collinearity Statistics		Adjusted R ²
		B	SE				Tolerance	VIF	
Daytime AT (n = 25)	(constant)	33.788	0.234		144.686	0.000			0.831
	DIST	0.002	0.000	0.876	10.417	0.000	0.996	1.004	
	FVC	-1.135	0.419	-0.228	-2.712	0.013	0.996	1.004	
Nighttime AT (n = 17)	(constant)	30.841	0.196		157.383	0.000			0.685
	DIST	0.001	0.000	0.973	5.969	0.000	0.742	1.347	
	FAR	0.081	0.021	0.640	3.927	0.002	0.742	1.347	
Daytime RH n = 19	(constant)	58.270	0.707		82.389	0.000			0.820
	DIST	-0.006	0.001	-0.890	-8.817	0.000	0.983	1.017	
	FVC	4.272	1.187	0.363	3.600	0.002	0.983	1.017	
Nighttime RH (n = 15)	(constant)	70.120	0.732		95.824	0.000			0.897
	DIST	-0.006	0.001	-1.005	-10.637	0.000	0.828	1.207	
	FAR	-0.226	0.074	-0.360	-3.062	0.011	0.534	1.874	
	FVC	2.262	0.765	0.329	2.958	0.013	0.597	1.676	
Daytime HI (n = 26)	(constant)	40.422	0.378		106.938	0.000			0.821
	DIST	0.003	0.000	0.897	10.602	0.000	1.000	1.000	
	FVC	-1.536	0.707	-0.184	-2.173	0.040	1.000	1.000	

Note: B means unstandardized coefficients; SE means standard error of the estimate; Standardized Coefficients means coefficients based on multiple linear regression with standardized input; t means t-value from a two-sided t-test; VIF means variance inflation factor.

4. Discussion

4.1. Cooling Effect of the Large River

Through mobile measurement, this study revealed that the large river had a great cooling effect on the surrounding built environment in the daytime and a weak cooling effect in the nighttime. For instance, during the daytime, the temperature reduction was up to 3.55 °C and the influence extended 1741 m away from the riverbank, which was much greater than most conclusions from previous studies [9,10,23]. In the nighttime, although previous studies observed very weak cooling of 0.37 °C in Seoul [23] and not evident cooling [9] or relative warming in Sheffield [10,13], we found slight but not negligible cooling with temperature reduction of 1.10 °C and influence distance of 1253 m. One possible reason is that the Yangtze River is the largest in China, with a river width of approximately 2 km near the survey routes. The huge heat capacity of the large river makes its temperature rise very slowly [66], so it still maintains a lower temperature than the urban surface at night.

Except for the cooling effect, the large river shows a humidifying effect at the same time. In the hot summer season, As the RH becomes higher, it makes it difficult for the skin surface to reduce temperature by evaporation of sweat [67], which may lead to thermal discomfort [35,68,69]. As a result, HI is a better index to assess the impact of waterbody on the littoral heat stress as it considers AT and RH simultaneously. This study found a great reduction in daytime HI and a slight increase in nighttime HI by the river. The daytime HI values of survey points were lower than the background HI of the city when within 1200 m from the riverbank. However, in the nighttime, HI values showed a trivial change in the littoral zone and HI was slightly higher than the background HI of the city. This meant that the benefits of AT cooling can offset the negative impact of humidifying during the daytime, but not in the nighttime. In addition, the daytime HI had a strong negative relation ($R^2 = 0.738$) with the distance from the riverbank. This is in line with the study in Shanghai [20], which claimed that urban waterbody can effectively improve thermal comfort and areas closer to the waterbody had greater benefits.

4.2. Influence of the Urban Built Environment

The influence of the urban built environment on water cooling effect cannot be ignored [66,70]. The microclimatic influence of the urban waterbody has been shown as the decrease in temperature and the increase in humidity in littoral areas. Our study confirmed temperature and humidity changes but revealed that the modification of the littoral thermal environment presents spatial anomaly by examining the HI–AT and HI–RH relations (shown in Figure 6) in the near-shore area, where the urban form was uneven. In other words, the built environment of the near-shore area, with much lower building coverage, resulted in higher daytime heat stress than expected. This finding highlighted the impact of the littoral built environment on cooling effect of the river.

In littoral areas with relatively moderate urban morphology, we found that the distance from the riverbank is one of the most influential factors affecting the water cooling effect, which was verified in the current literature [23,46]. Additionally, vegetation coverage was demonstrated to exert a second important impact (except for the distance) on AT, RH and HI, especially in the daytime. Our finding extended the understanding of cooling provision by urban greening, from playing a role in urban areas [32,35] and increasing water-cooling on the riverbank [9], to enhancing water cooling effect hundreds of meters away from the riverbank and contributing to mitigating heat stress at the pedestrian level during the daytime. In the nighttime, our findings implied that building morphology played a more important role than greening. It was consistent with the conclusion from Lan and Zhan [41] that most of the building–AT relations in Wuhan were significant during nighttime rather than the daytime. In detail, FAR entered two nighttime models in stepwise regressions and we found that a smaller FAR contributed to cooling and humidifying effects. This is because urban buildings would block the cold damp air from the river and a lower building volume can benefit to the propagation of cooling [71]. Additionally, FAR appeared to be an important variable in the nighttime models instead of the daytime models, possibly confirming the important thermal influence of the heat storage released at night from building materials [39,40,72,73]. According to the regression results, SVF did not have a significant impact on microclimate variables in this study, although it correlated significantly with FAR ($r = -0.747$). This may be because we only calculate SVF based on 3D building data and not involve the impact of street trees. Since FAR comprehensively measures the three-dimensional space occupation of buildings (Table 4), the impact of FAR on littoral microclimatic variables in our result was also the combined influence of building density and height.

4.3. Implications for Urban Planning and Design

China is making efforts to beat urban heat [74], aiming to build a climate-resilient society by 2035 and striving to preserve the green and blue spaces in urban areas [75]. There are many cities along the rivers, canals, lakes and coastal regions [45], which have the natural advantage of utilizing the cooling effects of the waterbody to mitigate urban heat stress during the summer days. It is warranted to understand the mutual impacts between the urban waterbody and the littoral built environment [76]. The findings of this study revealed the great potential of the large river for providing cooling benefits in summer daytime and contributing to mitigating pedestrian heat stress in littoral areas. For large rivers such as the Yangtze River, a microclimate-sensitive zone with a width of no less than 1 km or half of the river width, shall be set along the riverside. Climate-sensitive urban planning and design, including land-use planning, urban geometry design and urban greening, is warranted in this area. For example, green space is strongly recommended and street trees are also effective to enhance the water cooling effect. This offers urban residents the opportunity to benefit from cooling effect of blue and green spaces synthetically. Meanwhile, it should be noted that, despite the temperature reduction, rivers slightly increase pedestrian heat stress at night. Hence, the land-use type mainly used during the daytime, such as schools, hospitals and office buildings, are more favorable in

this area than the land-use type mainly occupied at night, such as residential buildings. In this area, the building form should be strictly controlled and the FAR is the primary index. Less densely distributed and moderately shorter buildings are conducive to the cooling extension of the large river. Those strategies for urban planners and designers would help to make good use of the cooling effect of the large river for UHI mitigation and support the building of climate-adaptive communities and climate-resilient cities.

4.4. Limitations and Future Research Directions

There are some limitations in this study to inspire future research. First, only one-day data was collected through mobile measurement and each round took 90 min in the morning and evening, respectively. Future studies are expected to involve a longer survey period and more data points to explore the thermal environment in the littoral zone of the urban river. Second, given the typically low background wind speed and relatively homogeneous built environment, this study mainly measured air temperature and relative humidity. Other microclimate variables (i.e., mean radiant temperature, specific humidity and wind conditions) are essential for measuring thermal comfort and their interactions with urban morphological factors [46]. Considering the complexity and dynamics of the urban environment, a comprehensive assessment of the littoral built environment, including more influential factors such as building materials, vegetation species, human behaviors, etc. [77], will deepen our understanding of the interaction between the water cooling effect and the littoral built environment. Third, as the cooling potential of a waterbody may vary across different seasons [66], it is warranted to investigate whether the findings in this study are consistent in other seasons. Additionally, as this study measured two routes in the same orientation, another possible direction is to include different street orientations in the future to investigate its impact on the extension of the water cooling effect [36].

5. Conclusions

We presented the spatial distribution of air temperature and relative humidity by mobile measurement and applied the heat index to assess pedestrian heat stress on a hot summer day near the Yangtze River. Thereafter, the relationships between the microclimatic variables and the urban built environment factors within the influence distances were analyzed. The main conclusions can be summarized as follows:

1. The large river showed great cooling and humidifying effect during the daytime. The temperature reduction was up to 3.55 °C with an influence distance of 1741 m away from the riverbank. The humidity increased up to 17.25% with an influence distance of 1369 m. In the nighttime, the cooling and humidifying effect still existed but was much weaker than daytime.
2. Considering both the influence of temperature and humidity, the river can significantly mitigate the pedestrian heat stress by reducing the heat index within 1200 m from the riverbank during the daytime but showed a weak negative effect in the nighttime.
3. A high level of vegetation cover in littoral areas can enhance water-cooling and humidifying and contribute to mitigating pedestrian heat stress during the daytime. Building morphology had a significant influence in the nighttime. Lower FAR could be beneficial for nighttime cooling and humidifying.

The analysis results of this study can provide suggestions for urban planning and design of littoral zones to better utilize the water cooling effect of urban waterbodies. Those strategies can be incorporated as part of mitigation and adaptation strategies.

Author Contributions: Conceptualization, Y.W. and W.O.; methodology, Y.W., W.O. and L.Z.; formal analysis, Y.W. and W.O.; writing—original draft preparation, Y.W.; writing—review and editing, Y.W., W.O., Q.Z. and L.Z.; funding acquisition, Y.W. and Q.Z.. All authors have read and agreed to the published version of the manuscript.

Funding: This research was funded by Zhejiang Provincial Natural Science Foundation of China under Grant No. LY20E080007; National Natural Science Foundation of China, Grant No. 52078389 and No. 51878515.

Institutional Review Board Statement: Not applicable.

Informed Consent Statement: Not applicable.

Data Availability Statement: Not applicable.

Conflicts of Interest: The authors declare no conflict of interest.

Appendix A

Table A1. Weather condition on the measurement day (21 July 2018).

Time (h)	AT (°C)	RH (%)	WS (m/s)	WD (°)
00:00	28.00	87	0.0	120
01:00	27.50	89	0.1	283
02:00	27.00	91	0.0	292
03:00	26.80	91	0.0	263
04:00	26.60	94	0.0	262
05:00	26.60	96	0.0	35
06:00	26.50	97	0.0	/*
07:00	29.40	89	0.6	59
08:00	33.00	65	1.9	127
09:00	34.50	57	2.3	135
10:00	35.60	53	2.1	102
11:00	36.20	51	1.8	99
12:00	36.60	49	2.1	215
13:00	37.10	47	0.5	288
14:00	37.60	44	2.5	333
15:00	38.10	44	2.8	9
16:00	38.40	41	2.5	6
17:00	38.00	43	2.4	3
18:00	37.30	45	1.6	346
19:00	35.10	54	1.3	356
20:00	33.20	64	1.3	10
21:00	33.50	64	3.3	32
22:00	32.90	62	4.1	42
23:00	31.70	66	2.6	28

* No data. Data source: <http://www.wunderground.com/> accessed on 21 July 2021.

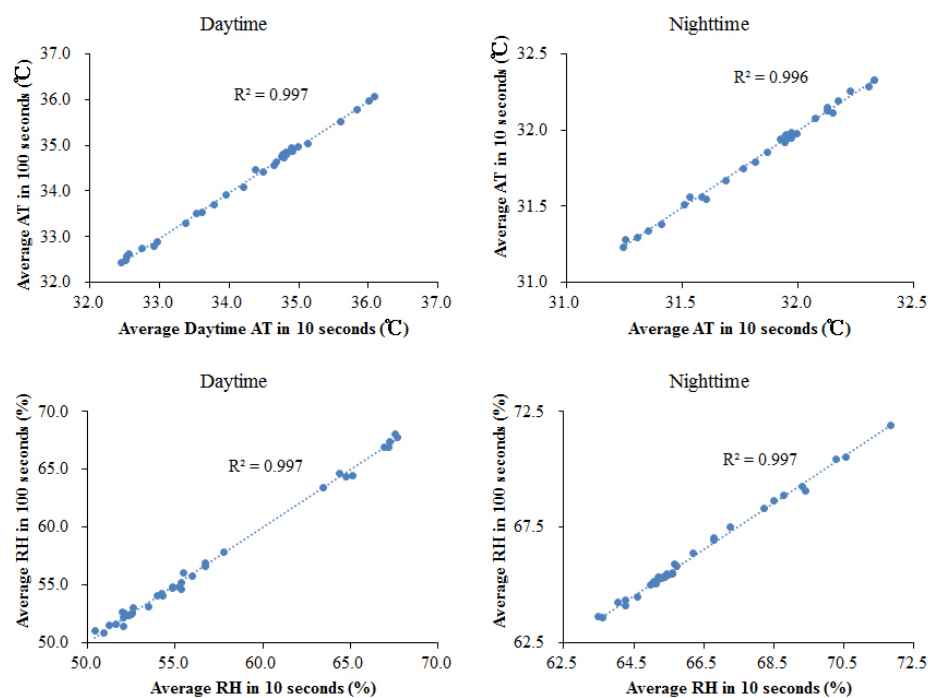


Figure A1. Correlations between these two periods were almost equal, with the R^2 above 0.99 and the slope nearly equal to 1.

References

1. IPCC. *Climate Change 2022: Impacts, Adaptation, and Vulnerability. Contribution of Working Group II to the Sixth Assessment Report of the Intergovernmental Panel on Climate Change*; Cambridge University Press: Cambridge, UK, 2022.
2. United Nations. *The World's Cities in 2018—Data Booklet (ST/ESA/SER.A/417)*. 2018. Available online: <https://www.un.org/development/desa/pd/content/worlds-cities-2018-data-booklet> (accessed on 8 August 2022).
3. Seto, K.C.; Golden, J.S.; Alberti, M.; Turner, B.L. Sustainability in an urbanizing planet. *Proc. Natl. Acad. Sci. USA* **2017**, *114*, 8935–8938. <https://doi.org/10.1073/pnas.1606037114>.
4. Masson, V.; Lemonsu, A.; Hidalgo, J.; Voogt, J. Urban Climates and Climate Change. *Annu. Rev. Environ. Resour.* **2020**, *45*, 411–444.
5. Sharifi, A. Co-benefits and synergies between urban climate change mitigation and adaptation measures: A literature review. *Sci. Total Environ.* **2021**, *750*, 141642. <https://doi.org/10.1016/j.scitotenv.2020.141642>.
6. Wang, Y.; Wang, A.; Zhai, J.; Tao, H.; Jiang, T.; Su, B.; Yang, J.; Wang, G.; Liu, Q.; Gao, C.; et al. Tens of thousands additional deaths annually in cities of China between 1.5 °C and 2.0 °C warming. *Nat. Commun.* **2019**, *10*, 3376. <https://doi.org/10.1038/s41467-019-11283-w>.
7. Gunawardena, K.R.; Wells, M.J.; Kershaw, T. Utilising green and bluespace to mitigate urban heat island intensity. *Sci. Total Environ.* **2017**, *584–585*, 1040–1055. <https://doi.org/10.1016/j.scitotenv.2017.01.158>.
8. Volker, S.; Baumeister, H.; Classen, T.; Hornberg, C.; Kistemann, T. Evidence for the temperature-mitigating capacity of urban blue space—A health geographic perspective. *Erdkunde* **2013**, *67*, 355–371. <https://doi.org/10.3112/erdkunde.2013.04.05>.
9. Hathway, E.A.; Sharples, S. The interaction of rivers and urban form in mitigating the Urban Heat Island effect: A UK case study. *Build. Environ.* **2012**, *58*, 14–22. <https://doi.org/10.1016/j.buildenv.2012.06.013>.
10. Tsai, C.W.; Young, T.; Warren, P.H.; Maltby, L. Riparian thermal conditions across a mixed rural and urban landscape. *Appl. Geogr.* **2017**, *87*, 106–114. <https://doi.org/10.1016/j.apgeog.2017.07.009>.
11. Moyer, A.N.; Hawkins, T.W. River effects on the heat island of a small urban area. *Urban Clim.* **2017**, *21*, 262–277. <https://doi.org/10.1016/j.uclim.2017.07.004>.
12. Heusinkveld, B.G.; Steeneveld, G.J.; van Hove, L.W.A.; Jacobs, C.M.J.; Holtslag, A.A.M. Spatial variability of the Rotterdam urban heat island as influenced by urban land use. *J. Geophys. Res. Atmos.* **2014**, *119*, 677–692. <https://doi.org/10.1002/2012jd019399>.
13. Murakawa, S.; Sekine, T.; Narita, K.I.; Nishina, D. Study of the effects of a river on the thermal environment in an urban area. *Energy Build.* **1991**, *16*, 993–1001. [https://doi.org/10.1016/0378-7788\(91\)90094-J](https://doi.org/10.1016/0378-7788(91)90094-J).
14. Wong, N.H.; Tan, C.L.; Nindyani, A.D.S.; Jusuf, S.K.; Tan, E. Influence of Water Bodies on Outdoor Air Temperature in Hot and Humid Climate. In *Proceedings of the International Conference on Sustainable Design & Construction (CSDC) 2011*, Kansas City, MO, USA, 23–25 March 2011; pp. 81–89. [https://doi.org/10.1061/41204\(426\)11](https://doi.org/10.1061/41204(426)11).

15. Wu, D.; Wang, Y.; Fan, C.; Xia, B. Thermal environment effects and interactions of reservoirs and forests as urban blue-green infrastructures. *Ecol. Indic.* **2018**, *91*, 657–663. <https://doi.org/10.1016/j.ecolind.2018.04.054>.
16. Gupta, N.; Mathew, A.; Khandelwal, S. Analysis of cooling effect of water bodies on land surface temperature in nearby region: A case study of Ahmedabad and Chandigarh cities in India. *Egypt. J. Remote Sens. Space Sci.* **2019**, *22*, 81–93. <https://doi.org/10.1016/j.ejrs.2018.03.007>.
17. Yu, K.; Chen, Y.H.; Liang, L.; Gong, A.; Li, J. Quantitative analysis of the interannual variation in the seasonal water cooling island (WCI) effect for urban areas. *Sci. Total Environ.* **2020**, *727*, 138750. <https://doi.org/10.1016/j.scitotenv.2020.138750>.
18. Wu, J.; Li, C.; Zhang, X.; Zhao, Y.; Liang, J.; Wang, Z. Seasonal variations and main influencing factors of the water cooling islands effect in Shenzhen. *Ecol. Indic.* **2020**, *117*, 106699. <https://doi.org/10.1016/j.ecolind.2020.106699>.
19. Tominaga, Y.; Sato, Y.; Sadohara, S. CFD simulations of the effect of evaporative cooling from water bodies in a micro-scale urban environment: Validation and application studies. *Sustain. Cities Soc.* **2015**, *19*, 259–270. <https://doi.org/10.1016/j.scs.2015.03.011>.
20. Xu, J.; Wei, Q.; Huang, X.; Zhu, X.; Li, G. Evaluation of human thermal comfort near urban waterbody during summer. *Build. Environ.* **2010**, *45*, 1072–1080. <https://doi.org/10.1016/j.buildenv.2009.10.025>.
21. Steeneveld, G.J.; Koopmans, S.; Heusinkveld, B.G.; Theeuwes, N.E. Refreshing the role of open water surfaces on mitigating the maximum urban heat island effect. *Landsc. Urban Plan.* **2014**, *121*, 92–96. <https://doi.org/10.1016/j.landurbplan.2013.09.001>.
22. Bowler, D.E.; Buyung-Ali, L.; Knight, T.M.; Pullin, A.S. Urban greening to cool towns and cities: A systematic review of the empirical evidence. *Landsc. Urban Plan.* **2010**, *97*, 147–155. <https://doi.org/10.1016/j.landurbplan.2010.05.006>.
23. Park, C.Y.; Lee, D.K.; Asawa, T.; Murakami, A.; Kim, H.G.; Lee, M.K.; Lee, H.S. Influence of urban form on the cooling effect of a small urban river. *Landsc. Urban Plan.* **2019**, *183*, 26–35. <https://doi.org/10.1016/j.landurbplan.2018.10.022>.
24. Tsin, P.K.; Knudby, A.; Krayenhoff, E.S.; Ho, H.C.; Brauer, M.; Henderson, S.B. Microscale mobile monitoring of urban air temperature. *Urban Clim.* **2016**, *18*, 58–72.
25. Qaid, A.; Bin Lamit, H.; Ossen, D.R.; Raja Shahminan, R.N. Urban heat island and thermal comfort conditions at micro-climate scale in a tropical planned city. *Energy Build.* **2016**, *133*, 577–595. <https://doi.org/10.1016/j.enbuild.2016.10.006>.
26. Yan, H.; Wu, F.; Dong, L. Influence of a large urban park on the local urban thermal environment. *Sci. Total Environ.* **2018**, *622–623*, 882–891. <https://doi.org/10.1016/j.scitotenv.2017.11.327>.
27. Ouyang, W.; Morakinyo, T.E.; Ren, C.; Liu, S.; Ng, E. Thermal-irradiant performance of green infrastructure typologies: Field measurement study in a subtropical climate city. *Sci. Total Environ.* **2021**, *764*, 144635. <https://doi.org/10.1016/j.scitotenv.2020.144635>.
28. Shi, Y.; Lau, K.L.; Ren, C.; Ng, E. Evaluating the local climate zone classification in high-density heterogeneous urban environment using mobile measurement. *Urban Clim.* **2018**, *25*, 167–186.
29. Leconte, F.; Bouyer, J.; Clavierie, R.; Pétrissans, M. Using Local Climate Zone scheme for UHI assessment: Evaluation of the method using mobile measurements. *Build. Environ.* **2015**, *83*, 39–49. <https://doi.org/10.1016/j.buildenv.2014.05.005>.
30. Liu, Z.; Cheng, K.; He, Y.; Jim, C.Y.; Brown, R.; Shi, Y.; Lau, K.; Ng, E. Microclimatic measurements in tropical cities: Systematic review and proposed guidelines. *Build. Environ.* **2022**, *222*, 109411. <https://doi.org/10.1016/j.buildenv.2022.109411>.
31. Cheung, P.; Jim, C. Comparing the cooling effects of a tree and a concrete shelter using PET and UTCI. *Build. Environ.* **2017**, *130*, 49–61.
32. Demuzere, M.; Orru, K.; Heidrich, O.; Olazabal, E.; Geneletti, D.; Orru, H.; Bhave, A.; Mittal, N.; Feliu, E.; Faehnle, M. Mitigating and adapting to climate change: Multi-functional and multi-scale assessment of green urban infrastructure. *J. Environ. Manag.* **2014**, *146*, 107–115.
33. Ng, E.; Chen, L.; Wang, Y.N.; Yuan, C. A study on the cooling effects of greening in a high-density city: An experience from Hong Kong. *Build. Environ.* **2012**, *47*, 256–271. <https://doi.org/10.1016/j.buildenv.2011.07.014>.
34. Ouyang, W.; Morakinyo, T.E.; Ren, C.; Ng, E. The cooling efficiency of variable greenery coverage ratios in different urban densities: A study in a subtropical climate. *Build. Environ.* **2020**, *174*, 106772. <https://doi.org/10.1016/j.buildenv.2020.106772>.
35. Cheung, P.K.; Jim, C.Y. Effects of urban and landscape elements on air temperature in a high-density subtropical city. *Build. Environ.* **2019**, *164*, 106362. <https://doi.org/10.1016/j.buildenv.2019.106362>.
36. Jamei, E.; Rajagopalan, P.; Seyedmahmoudian, M.; Jamei, Y. Review on the impact of urban geometry and pedestrian level greening on outdoor thermal comfort. *Renew. Sust. Energ. Rev.* **2016**, *54*, 1002–1017. <https://doi.org/10.1016/j.rser.2015.10.104>.
37. Yin, C.; Yuan, M.; Lu, Y.; Huang, Y.; Liu, Y. Effects of urban form on the urban heat island effect based on spatial regression model. *Sci. Total Environ.* **2018**, *634*, 696–704. <https://doi.org/10.1016/j.scitotenv.2018.03.350>.
38. Yang, F.; Lau, S.S.Y.; Qian, F. Urban design to lower summertime outdoor temperatures: An empirical study on high-rise housing in Shanghai. *Build. Environ.* **2011**, *46*, 769–785. <https://doi.org/10.1016/j.buildenv.2010.10.010>.
39. Oke, T.R.; Mills, G.; Christen, A.; Voogt, J.A. *Urban Climates*; Cambridge University Press: Cambridge, UK, 2017. <https://doi.org/10.1017/9781139016476>.
40. Yan, H.; Fan, S.; Guo, C.; Wu, F.; Zhang, N.; Dong, L. Assessing the effects of landscape design parameters on intra-urban air temperature variability: The case of Beijing, China. *Build. Environ.* **2014**, *76*, 44–53. <https://doi.org/10.1016/j.buildenv.2014.03.007>.

41. Lan, Y.; Zhan, Q. How do urban buildings impact summer air temperature? The effects of building configurations in space and time. *Build. Environ.* **2017**, *125*, 88–98. <https://doi.org/10.1016/j.buildenv.2017.08.046>.
42. Perini, K.; Magliocco, A. Effects of vegetation, urban density, building height, and atmospheric conditions on local temperatures and thermal comfort. *Urban For. Urban Green.* **2014**, *13*, 495–506. <https://doi.org/10.1016/j.ufug.2014.03.003>.
43. Liu, L.; Lin, Y.; Liu, J.; Wang, L.; Wang, D.; Shui, T.; Chen, X.; Wu, Q. Analysis of local-scale urban heat island characteristics using an integrated method of mobile measurement and GIS-based spatial interpolation. *Build. Environ.* **2017**, *117*, 191–207. <https://doi.org/10.1016/j.buildenv.2017.03.013>.
44. Zhao, C.; Fu, G.; Liu, X.; Fu, F. Urban planning indicators, morphology and climate indicators: A case study for a north-south transect of Beijing, China. *Build. Environ.* **2011**, *46*, 1174–1183. <https://doi.org/10.1016/j.buildenv.2010.12.009>.
45. Hu, L.Q.; Li, Q. Greenspace, bluespace, and their interactive influence on urban thermal environments. *Environ. Res. Lett.* **2020**, *15*, 034041. <https://doi.org/10.1088/1748-9326/ab6c30>.
46. Manteghi, G. Influence of Street Orientation and Distance To Water Body on Microclimate Temperature Distribution In Tropical Coastal City of Malacca. *Int. J. Appl. Environ. Sci.* **2015**, *10*, 749–766.
47. Katayama, T.; Hayashi, T.; Shiotsuki, Y.; Kitayama, H.; Ishii, A.; Nishida, M.; Tsutsumi, J.I.; Oguro, M. Cooling effects of a river and sea breeze on the thermal environment in a built-up area. *Energy Build.* **1991**, *16*, 973–978.
48. Schwarz, N.; Schlink, U.; Franck, U.; Großmann, K. Relationship of land surface and air temperatures and its implications for quantifying urban heat island indicators—An application for the city of Leipzig (Germany). *Ecol. Indic.* **2012**, *18*, 693–704. <https://doi.org/10.1016/j.ecolind.2012.01.001>.
49. Charabi, Y.; Bakhit, A. Assessment of the canopy urban heat island of a coastal arid tropical city: The case of Muscat, Oman. *Atmos. Res.* **2011**, *101*, 215–227. <https://doi.org/10.1016/j.atmosres.2011.02.010>.
50. Steadman, R.G. The Assessment of Sultriness. Part I: A Temperature-Humidity Index Based on Human Physiology and Clothing Science. *J. Appl. Meteorol.* **1979**, *18*, 861. [https://doi.org/10.1175/1520-0450\(1979\)018<0861:TAOSPI>2.0.CO;2](https://doi.org/10.1175/1520-0450(1979)018<0861:TAOSPI>2.0.CO;2).
51. Anderson, G.B.; Bell, M.L.; Peng, R.D. Methods to Calculate the Heat Index as an Exposure Metric in Environmental Health Research. *Environ. Health Perspect.* **2013**, *121*, 1111–1119.
52. Davis, R.E.; Knappenberger, P.C.; Michaels, P.J.; Novicoff, W.M. Changing heat-related mortality in the United States. *Environ. Health Perspect.* **2003**, *111*, 1712–1718. <https://doi.org/10.1289/ehp.6336>.
53. Wu, D. Environmental Meteorology and Special Meteorological Forecasts. *Meteorol. Mon.* **2000**, *26*, 3–5.
54. Ahrens, C.D. *Essentials of Meteorology: An Invitation to the Atmosphere*; Cengage Learning: Boston, MA, USA, 2010.
55. Hass, A.L.; Ellis, K.N.; Reyes Mason, L.; Hathaway, J.M.; Howe, D.A. Heat and Humidity in the City: Neighborhood Heat Index Variability in a Mid-Sized City in the Southeastern United States. *Int. J. Environ. Res. Public Health* **2016**, *13*, 117.
56. NOAA. Available online: https://www.wpc.ncep.noaa.gov/html/heatindex_equation.shtml (accessed on 24 May 2022).
57. Jiang, Z.; Huete, A.R.; Jin, C.; Chen, Y.; Jing, L.; Yan, G.; Zhang, X. Analysis of NDVI and scaled difference vegetation index retrievals of vegetation fraction. *Remote Sens. Environ.* **2006**, *101*, 366–378.
58. Gutman, G.; Ignatov, A. The derivation of the green vegetation fraction from NOAA/AVHRR data for use in numerical weather prediction models. *Int. J. Remote Sens.* **1998**, *19*, 1533–1543.
59. Xu, Y.; Ren, C.; Ma, P.; Ho, J.; Wang, W.; Lau, K.K.-L.; Lin, H.; Ng, E. Urban morphology detection and computation for urban climate research. *Landsc. Urban Plan.* **2017**, *167*, 212–224.
60. Edussuriya, P.; Chan, A.; Ye, A. Urban morphology and air quality in dense residential environments in Hong Kong. Part I: District-level analysis. *Atmos. Environ.* **2011**, *45*, 4789–4803. <https://doi.org/10.1016/j.atmosenv.2009.07.061>.
61. Yang, F.; Qian, F.; Lau, S.S.Y. Urban form and density as indicators for summertime outdoor ventilation potential: A case study on high-rise housing in Shanghai. *Build. Environ.* **2013**, *70*, 122–137. <https://doi.org/10.1016/j.buildenv.2013.08.019>.
62. Yang, F.; Lau, S.S.Y.; Qian, F. Summertime heat island intensities in three high-rise housing quarters in inner-city Shanghai China: Building layout, density and greenery. *Build. Environ.* **2010**, *45*, 115–134. <https://doi.org/10.1016/j.buildenv.2009.05.010>.
63. Merbitz, H.; Fritz, S.; Schneider, C. Mobile measurements and regression modeling of the spatial particulate matter variability in an urban area. *Sci. Total Environ.* **2012**, *438*, 389–403. <https://doi.org/10.1016/j.scitotenv.2012.08.049>.
64. Bernard, J.; Bocher, E.; Petit, G.; Palominos, S. Sky View Factor Calculation in Urban Context: Computational Performance and Accuracy Analysis of Two Open and Free GIS Tools. *Climate* **2018**, *6*, 60.
65. Peng, J.; Dan, Y.; Qiao, R.; Liu, Y.; Dong, J.; Wu, J. How to quantify the cooling effect of urban parks? Linking maximum and accumulation perspectives. *Remote Sens. Environ.* **2021**, *252*, 112135. <https://doi.org/10.1016/j.rse.2020.112135>.
66. Wang, Y.; Ouyang, W. Investigating the heterogeneity of water cooling effect for cooler cities. *Sustain. Cities Soc.* **2021**, *75*, 103281. <https://doi.org/10.1016/j.scs.2021.103281>.
67. Sobolewski, A.; Młynarczyk, M.; Konarska, M.; Bugajska, J. The influence of air humidity on human heat stress in a hot environment. *Int. J. Occup. Saf. Ergon.* **2021**, *27*, 226–236. <https://doi.org/10.1080/10803548.2019.1699728>.
68. Imam Syafii, N.; Ichinose, M.; Kumakura, E.; Jusuf, S.K.; Chigusa, K.; Wong, N.H. Thermal environment assessment around bodies of water in urban canyons: A scale model study. *Sustain. Cities Soc.* **2017**, *34*, 79–89. <https://doi.org/10.1016/j.scs.2017.06.012>.

69. Amani-Beni, M.; Zhang, B.; Xie, G.-d.; Xu, J. Impact of urban park's tree, grass and waterbody on microclimate in hot summer days: A case study of Olympic Park in Beijing, China. *Urban For. Urban Green.* **2018**, *32*, 1–6. <https://doi.org/10.1016/j.ufug.2018.03.016>.
70. Cheng, L.; Guan, D.; Zhou, L.; Zhao, Z.; Zhou, J. Urban cooling island effect of main river on a landscape scale in Chongqing, China. *Sustain. Cities Soc.* **2019**, *47*, 101501. <https://doi.org/10.1016/j.scs.2019.101501>.
71. Ng, E.; Yuan, C.; Chen, L.; Ren, C.; Fung, J.C.H. Improving the wind environment in high-density cities by understanding urban morphology and surface roughness: A study in Hong Kong. *Landsc. Urban Plan.* **2011**, *101*, 59–74. <https://doi.org/10.1016/j.landurbplan.2011.01.004>.
72. Chow, W.T.L.; Roth, M. Temporal dynamics of the urban heat island of Singapore. *Int. J. Climatol.* **2006**, *26*, 2243–2260. <https://doi.org/10.1002/joc.1364>.
73. Masson, V. A physically-based scheme for the urban energy budget in atmospheric models. *Bound. Layer Meteorol.* **2000**, *94*, 357–397.
74. He, B.-J.; Wang, J.; Zhu, J.; Qi, J. Beating the urban heat: Situation, background, impacts and the way forward in China. *Renew. Sustain. Energy Rev.* **2022**, *161*, 112350. <https://doi.org/10.1016/j.rser.2022.112350>.
75. Chinese Ministry of Ecology and Environment; National Development and Reform Commission; Ministry of Science and Technology; Ministry of Finance; Ministry of Natural Resources; Ministry of Housing and Urban-Rural Development; Ministry of Transport; Ministry of Water Resources; Ministry of Agriculture and Rural Affairs; Ministry of Culture and Tourism; National Health Commission; Ministry of Emergency Management; People's Bank of China; Chinese Academy of Sciences; China Meteorological Administration; National Energy Administration; National Forestry and Grassland Administration. *National Climate Change Adaptation Strategy 2035*; Ministry of Ecology and Environment of the People's Republic of China: Beijing, China, 2022.
76. Liu, H.; Huang, B.; Zhan, Q.; Gao, S.; Li, R.; Fan, Z. The influence of urban form on surface urban heat island and its planning implications: Evidence from 1288 urban clusters in China. *Sustain. Cities Soc.* **2021**, *71*, 102987. <https://doi.org/10.1016/j.scs.2021.102987>.
77. Bassolino, E.; D'Ambrosio, V.; Sgobbo, A. Data Exchange Processes for the Definition of Climate-Proof Design Strategies for the Adaptation to Heatwaves in the Urban Open Spaces of Dense Italian Cities. *Sustainability* **2021**, *13*, 5694.